

Magnetic domain structure within half-metallic ferromagnetic kagome compound $\text{Co}_3\text{Sn}_2\text{S}_2$ Akira Sugawara^{1,*}, Tetsuya Akashi,¹ Mohamed A. Kassem,^{2,†} Yoshikazu Tabata,² Takeshi Waki,² and Hiroyuki Nakamura²¹Center for Exploratory Research Laboratory, Hitachi, Ltd, Hatoyama, Saitama 350-0395, Japan²Department of Materials Science and Engineering, Kyoto University, Kyoto, 606-8501, Japan

(Received 27 March 2019; published 30 October 2019)

$\text{Co}_3\text{Sn}_2\text{S}_2$ has been attracting attention as a model quasi-2D kagome ferromagnet as well as a ferromagnetic Weyl semimetal. Here, we report the evolution of the magnetic domain within $\text{Co}_3\text{Sn}_2\text{S}_2$ as a function of temperature and external field as studied by *in situ* Lorentz microscopy. The domain structure typical for anisotropy-controlled material was observed, and domain wall (DW) motion was found to depend strongly on temperature. It was inactive due to strong pinning in a low-temperature range yet activated as a result of thermal depinning with increasing temperature. The activation temperature decreased as the external field increased. In the temperature range just below the Curie temperature, spontaneous domain reorganization associated with DW creep occurred even in the absence of an external field. The low-field anomalous magnetic phase just below the Curie temperature and split between zero-field-cooled and field-cooled magnetization-temperature curves found in our previous study [M. A. Kassem *et al.*, *Phys. Rev. B* **96**, 014429 (2017)] are explained in terms of temperature-dependent DW motion including the DW creep.

DOI: [10.1103/PhysRevMaterials.3.104421](https://doi.org/10.1103/PhysRevMaterials.3.104421)

I. INTRODUCTION

$\text{Co}_3\text{Sn}_2\text{S}_2$ is a typical half-metallic ferromagnetic compound that has a shandite-type structure [1–11]. In the structure, Co atoms are arranged on a two-dimensional kagome lattice with an in-plane Co-Co distance of 0.27 nm. The layers involving Co are separated by a Sn-S block with an interlayer distance of 0.44 nm [1]. The compound exhibits interesting magnetic properties originating from its quasi-two-dimensional nature. Furthermore, it has attracted attention as a model magnetic Weyl semimetal [8–10]. We previously measured the temperature-dependent magnetization and alternative-current susceptibility and reported three important features of this compound: the occurrence of anomalous magnetic phase (hereafter A phase) at low field and just below the Curie temperature ($T_c = 175$ K), large splits of magnetization curves between field-cooled (FC) and zero-field-cooled (ZFC) at low field, and extremely slow spin dynamics with relaxation times longer than 10 s [7]. The FC/ZFC curve split was also reported by another group (in Supplemental material of Ref. [10]). Such a low-field anomaly may originate from magnetic domain structures or novel spin textures. An example of such textures stabilized in a finite magnetic field and just below T_c is skyrmion, which is a whirl-like spin texture topologically stabilized under the existence of Dzyaloshinskii-Moriya (DM) interaction [12]. Rich variation in spin texture including skyrmion was also reported for a non-DM uniaxial ferromagnet with dipolar contribution [13]. A similar type of spin texture, “skyrmionic bubble,” was re-

ported for another kagome compound, Fe_3Sn_2 [14], of which the easy axis canted from the c axis depending on temperature [15]. The compound is also interesting as a massive Dirac fermion system [16].

The variation in micromagnetic structure depending on external field (H) and temperature (T) is the main focus of this study [17]. The saturation magnetization M_s of $\text{Co}_3\text{Sn}_2\text{S}_2$ is very small, 0.098 T ($\sim 0.28 \mu_B/\text{Co}$) at 2 K. Exchange stiffness A has not been determined experimentally. Due to the two-dimensional nature of the compound, exchange within kagome layers is expected to differ from interlayer exchange. The compound exhibits strong uniaxial anisotropy with the easy axis parallel to the crystallographic c axis. Anisotropy field H_A was reported to be at least greater than the maximum field of commercial SQUID equipment (5–8 T) even just below T_c [10,11]. Although H_A and its temperature dependence have not been determined, uniaxial anisotropy energy, $K_u = H_A/2M_s$, is considered to be extremely large. No report has been made on DM interaction for this compound having centrosymmetry. Due to the contributions of small demagnetization energy and large uniaxial anisotropy energy, the micromagnetic structure of $\text{Co}_3\text{Sn}_2\text{S}_2$ is considered to be anisotropy-controlled. The typical domain structure of such materials with strong uniaxial magnetocrystalline anisotropy is a stripe domain accompanied with 180° Bloch domain walls (DWs). Magnetic domain observation by Lorentz microscopy is powerful for analyzing such micromagnetic structures at high resolution [17]. In this study, we present the experimental results of Lorentz microscopy for $\text{Co}_3\text{Sn}_2\text{S}_2$ as a function of external field and temperature.

II. EXPERIMENTAL

The main difficulty of observing $\text{Co}_3\text{Sn}_2\text{S}_2$ is its small magnetization, especially in a temperature range at which the

*Present address: Center for Exploratory Research Laboratory, Hitachi, Ltd, Akanuma 2520, Saitama 350-0395, Japan; akira.sugawara.ne@hitachi.com

†Present address: Department of Physics, Faculty of Science, Assiut University, 71516 Assiut, Egypt.

A phase is expected to appear just below T_c . To detect small electron phase changes by Lorentz microscopy, we observed low-defect, thick specimens with an ultra-high-voltage (1MV) cold-field-emission transmission electron microscope (TEM) [18], which was successfully used to observe (Ga, Mn)As with its M_s as small as 0.02 T [19]. We observed several electron-transparent specimens prepared by using a focused ion beam (FIB) method from a single crystal $\text{Co}_3\text{Sn}_2\text{S}_2$ grown with the Bridgman method, including out-of-plane specimens (with its c axis perpendicular to the planes) and also in-plane specimens (with its c axis laid in the plane). To avoid ion damage on the sulphide surface, finishing was performed at a low ion voltage (10 kV). Note that domain contrast was not observed clearly when the specimen thickness was smaller than roughly 150 nm. The results presented in this paper was obtained for one of the out-of-plane specimens with a $15 \times 15 \mu\text{m}$ field of view and a 300 nm thickness approximately. A double-tilt liquid-helium-cooling specimen holder was used in this experiment. The specimen tilt was used to induce magnetization component perpendicular to the beam path to cause Lorentz deflection, and also to reduce diffraction contrast that may mask the DW contrast. The temperature was controlled by using a semiconductor sensor and a proportional-integral-differential (PID) controller. The difference between the sensor read-out and actual specimen temperature was estimated to be as large as 15° when the read-out was below 10 K and within a few degrees near the T_c of $\text{Co}_3\text{Sn}_2\text{S}_2$. The temperature error may have also been large even at high temperature when the cooling/heating rate was large. The Lorentz images were acquired by using a slow-scan coupled-charge device (CCD) camera at an underfocus condition with defocus value of -63 nm. The defocus amount was fixed during continuous acquisition of a series of Lorentz images with varying temperature. When the specimen temperature was changed, the specimen drift occurred. Most of the individual images shown in this paper were accumulations of, generally, five $2\text{k} \times 2\text{k}$ images with an exposure time of 2 sec after the drift became negligible. To the contrary, small-size ($1\text{k} \times 1\text{k}$) images were acquired continuously when the measurement was performed at a constant temperature change rate. In-situ observation under a magnetic field was done with a magnetizing device composed of three pairs of superconducting Helmholtz coils [20]. The device and specimen were located between a conventional objective lens and the illumination system of the microscope. A weakly excited objective lens was used as a long-focal imaging lens, and its stray field was smaller than 1 Oe at the specimen position. In this experiment, external field H up to 500 Oe was applied parallel to the electron beam path, i.e., nearly parallel to the uniaxial easy axis of the out-of-plane $\text{Co}_3\text{Sn}_2\text{S}_2$ specimen. The in-plane field component is estimated nearly 30% of the applied field. Such in-plane field much smaller than the anisotropy field of $\text{Co}_3\text{Sn}_2\text{S}_2$ is not thought to influence the domain motion significantly. We confirmed that the significant domain wall motion did not occur when the 100 Oe field was applied perpendicular to the electron beam path, and the temperature was varied from 50 to 180 K.

III. RESULTS

A. Domain evolution with temperature varied at $H = 100 - 500$ Oe

A series of Fresnel-mode Lorentz DW images were acquired for an out-of-plane specimen with temperature varied across T_c when $H = 300$ Oe was applied parallel to the electron beam path (Fig. 1). The Lorentz DW contrast was visible only when the specimen normal was tilted, roughly $15^\circ - 20^\circ$, from the beam direction. The specimen tilt was required to induce magnetization component perpendicular to the beam path. The result indicates that spontaneous magnetization was parallel to the c axis, and that the DWs situated in between the magnetic domains with upward and downward magnetization. From the Lorentz images, we can determine the volume of the domain polarized parallel (V_\uparrow) and antiparallel (V_\downarrow) to the external field and its ratio [$V_r = V_\uparrow / (V_\uparrow + V_\downarrow)$]. For the single crystal with uniaxial magnetocrystalline anisotropy, V_r is related to the magnetization (M) and saturation magnetization (M_s) in the following form:

$$V_r(H, T) = \frac{V_\uparrow(H, T)}{V_\uparrow(H, T) + V_\downarrow(H, T)} = \frac{M(H, T)}{M_s(T)} + 0.5. \quad (1)$$

Although the Lorentz contrast due to in-plane magnetization within the DWs was observed frequently when the beam was exactly parallel to the easy axis [13], we could not resolve the DW images in such geometry. The DW width, $2\sqrt{A/K_u}$, was probably so small that we could not resolve it under large defocus required for DW imaging in materials with such small M_s .

We first cooled the specimen rapidly through T_c down to below 12 K under $H = 0$ to develop maze domain as a thermally-demagnetized state [Fig. 1(a)]. Next, the field increased up to 300 Oe at this temperature [Fig. 1(b)]. The DWs motion occurred only in the region marked by a dotted oval in Fig. 1(a). The change in V_r was very small. The result indicates strong DW pinning at such low temperature. Subsequently, the specimen temperature increased under the fixed field [Figs. 1(b)–1(o)]. The DW contrast weakened as the temperature increased, indicating that the local moment monotonically decreased as the temperature increased. The DWs were found to rarely move below 119 K [Fig. 1(b)–1(g)]. In such temperature range, the DW motion occurred mainly to eliminate the DWs with small curvature such like narrow noses extending from large domains and small round domains as seen in the regions marked by dotted ovals. Such morphological change in DWs is expected to reduce total micromagnetic energy effectively, although it is not accompanied with significant change in M . Due to large K_u and small M_s , misalignment of the spins from the easy axis is expected to occur predominantly in the DWs. Therefore the domain wall energy (proportional to the length of the line DW images) is a dominant micromagnetic energy of this system, whereas the demagnetization energy determined by arrangement of the surface poles is less important. The round shape minimizes DW energy for a given domain volume.

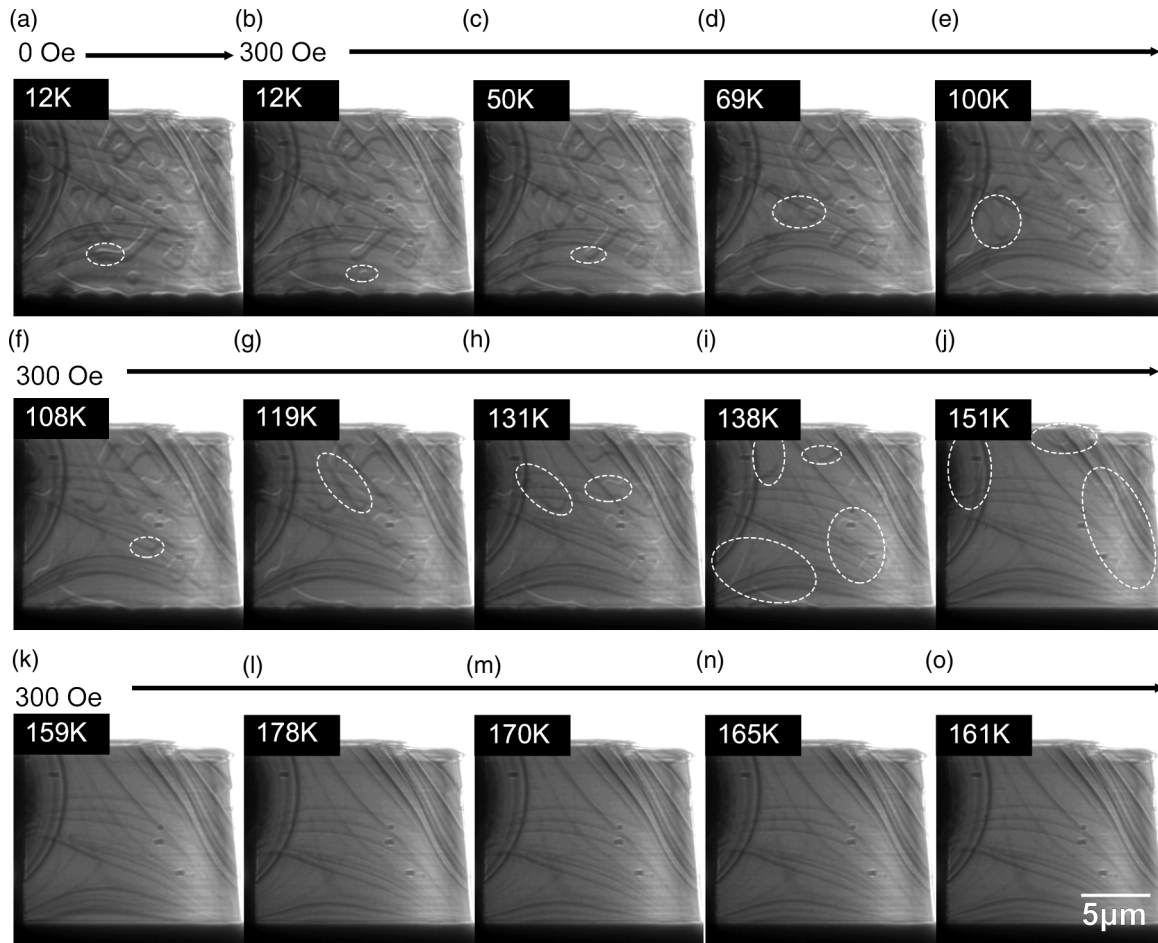


FIG. 1. Temperature-dependent magnetic domain evolution in external field $H = 300$ Oe. (a) The specimen was cooled down to 12 K under zero field, and (b) H was increased to 300 Oe at 12 K. Then the temperature was increased at $H = 300$ Oe from (b) 12 to (l) 178 K across T_c , and then cooled down to (o) 161 K across T_c . Two different types of image contrast coexist in images; one is magnetic DW image (seen as black and white lines), and other is bend contours (seen as dark broad bands) associated with diffraction contrast. Bend contours can be distinguished from DW images because crystallographic contrast remained visible above T_c , and their shape and position varied with temperature according to thermal specimen deformation. The DW motion occurred in the areas marked by dotted ovals during the transition to the next frames.

In contrast, the DW motion activated in the range 119 K [Fig. 1(g)] $< T < 159$ K [Fig. 1(k)] was accompanied with drastic change of net magnetization (M). The domains with magnetization antiparallel to the field shrunk as the field increased. The DWs moved more easily at high temperature because the DW depinning was enhanced thermally. The DWs were regarded as stationary in the duration time (10 seconds). The results imply that DW motion is discontinuous-intermittent motion due to repeated thermal depinning and repinning at another pinning center. However, the DW pinning sites could not be related to crystal defects visible in the present image resolution. The field of view eventually turned into a single domain as a result of all DWs being swept out at around 159 K [Fig. 1(k)]. The specimen was heated further to the temperature above T_c [Fig. 1(l)], and then cooled down across T_c . The single domain state developed immediately below T_c as evidenced by no DW contrast during cooling down to 161 K [Figs. 1(l)–1(o)].

The DW motion was dependent of external field H . Figure 2 shows a series of Fresnel-mode Lorentz DW images

of the specimen when the temperature was raised at $H = 100$ Oe. As in the case of 300 Oe (Fig. 1), the DW motion did not occur when the H was increased from 0 to 100 Oe at 12 K [Figs. 2(a) and 2(b)]. The DW motion rarely occurred until the temperature reached up to 140 K [Figs. 2(c) and 2(d)]. The extensive DW motion occurred in very narrow temperature range [160 K (Fig. 2(e)) $< T < 172$ K [Fig. 2(h)]. The results indicate that enhanced thermal agitation is required to cause the DW depinning as the external field decreases. We also confirmed that the DW formation did not occur when another specimen was cooled down at $H = 100$ Oe.

Figure 3 shows a series of Lorentz DW images of the specimen when the temperature was raised at $H = 500$ Oe, which was the maximum applied field in this study. Again, the DW motion did not occur even when the H was increased from 0 to 500 Oe at 10 K [Figs. 3(a) and 3(b)]. Since the external field increased, the DW motion occurred at lower temperature than the case of $H = 100$ and 300 Oe. The DW motion below 75 K [Figs. 3(b)–3(d)] occurred mainly to eliminate

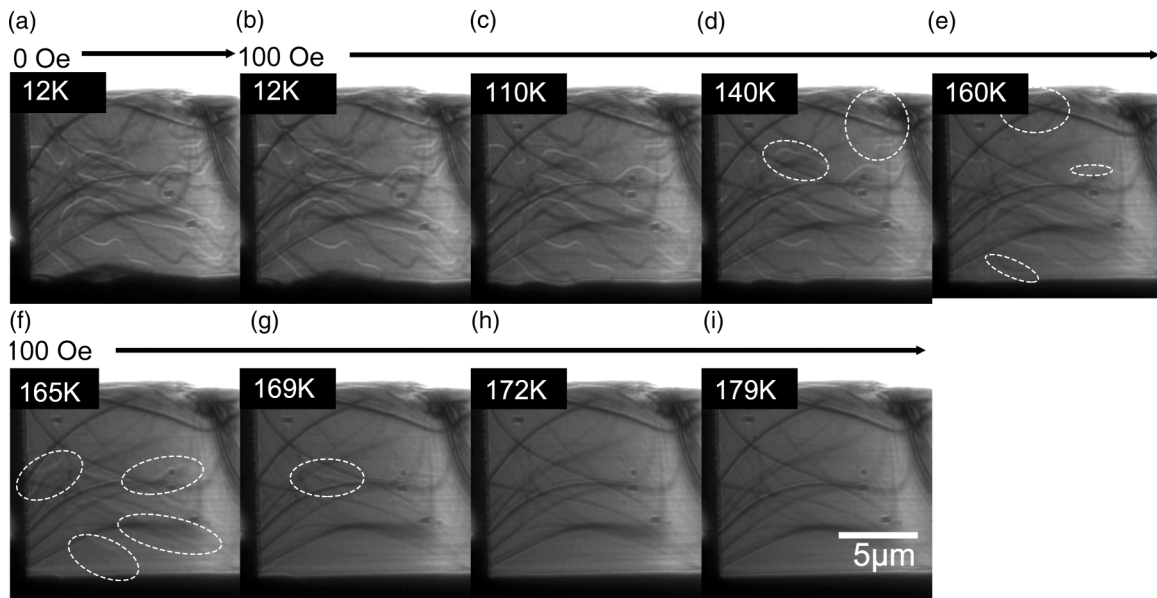


FIG. 2. Temperature-dependent magnetic domain evolution in external field $H = 100$ Oe. (a) The specimen was cooled down to 12 K under zero field, and (b) H was increased to 100 Oe at 12 K. Then the temperature was increased at $H = 100$ Oe from (b) 12 to (i) 179 K across T_c . The DW motion occurred in the areas marked by dotted ovals during the transition to the next frames.

narrow noses or to collapse small round domains. The net magnetization (M) changed significantly in the range $75 \text{ K} < T < 130 \text{ K}$ [Figs. 3(d)–3(h)] by the activated DW motion. All DWs were swept out at around 147 K [Fig. 3(i)], and the field of view turned into a single domain. The temperature range in which extensive DW motion occurred shifted toward lower temperature as the external field increased. (The domain evolution upon specimen heating at $H = 100, 300,$ and 500 Oe was also shown in movie format [21])

Figure 4 shows V_r as a function of T and H . The specimen was nearly demagnetized (V_r is nearly 0.5) at low temperature, whereas V_r increases rapidly after thermal depinning of the DWs occurred. The temperature range in which DW motion was activated shifts toward a higher temperature as H decreased. Note that thermal depinning was also observed for an in-plane specimen when $H = 100$ Oe was applied parallel to the c axis (images not shown here) in a similar temperature range (150–160 K).

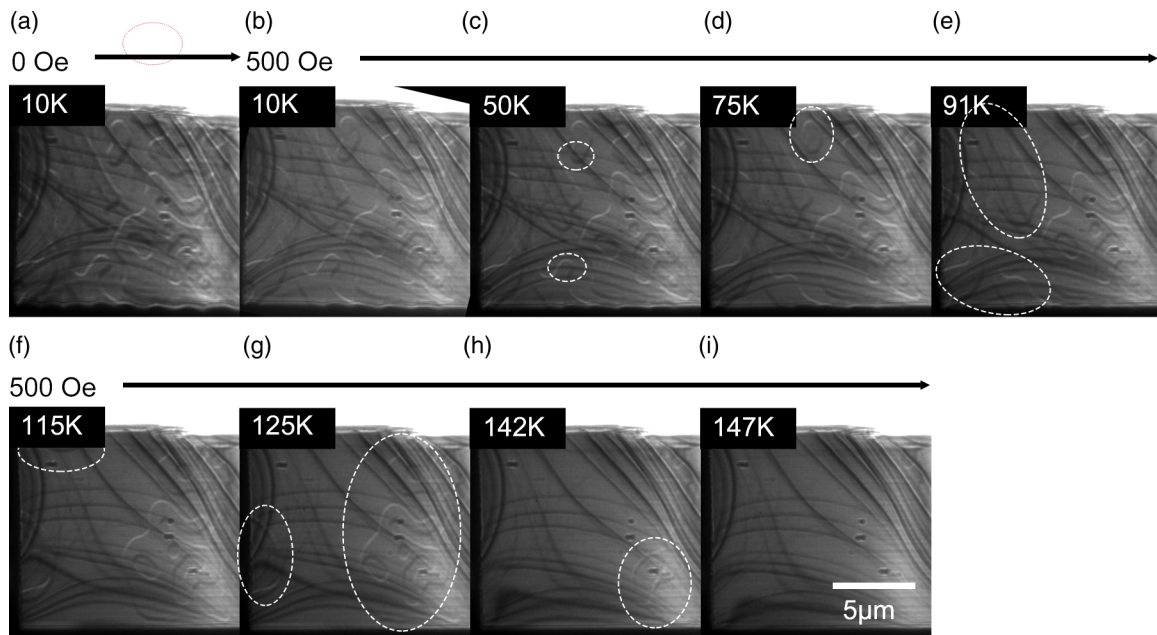


FIG. 3. Temperature-dependent magnetic domain evolution in external field $H = 500$ Oe. (a) The specimen was cooled down to 10 K under zero field, and (b) H was increased to 500 Oe at 12 K. Then the temperature was increased at $H = 500$ Oe from (b) 10 to (i) 147 K. The DW motion occurred in the areas marked by dotted ovals during the transition to the next frames.

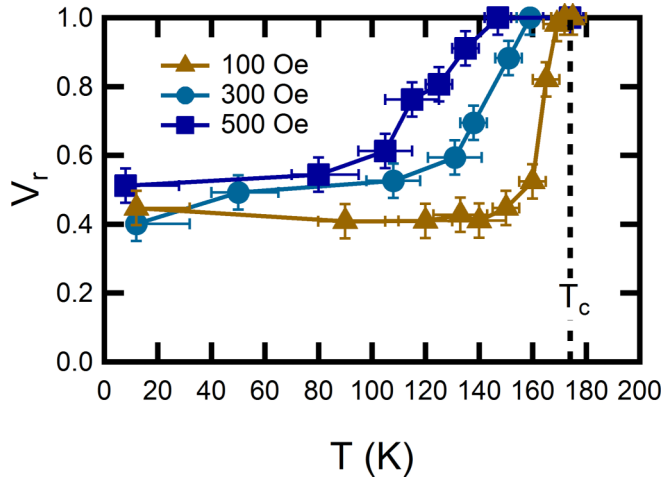


FIG. 4. Temperature- and external-field dependence of volume fraction of domains polarized parallel to external field.

B. Domain evolution with varying temperature at $H = 0$

Domain evolution occurred quite differently when $H = 0$. A series of selected Lorentz micrographs obtained while raising the temperature is shown in Fig. 5. (A full set of the images was shown in Ref. [21].) We performed image subtraction in order to extract weak DW contrast above 160 K [21]. The DWs had remained unchanged below 171 K during heating [Figs. 5(a)–5(d)]. However, the DW motion was activated in very narrow temperature range between 171 and 173 K. The prominent feature was that the coarse maze domains became reorganized into fine maze domains according to the active DW motion [Figs. 5(d)–5(f)]. Subsequently,

the domain contrast became undetectable at 174 K [Fig. 5(g)]. It is surprising that the spontaneous refinement of the domain occurred in the absence of the external field. It should be noted that the DW energy, which is proportional to DW area, increased as a result of the refinement.

Next, we show the domain evolution during the cooling through T_c in Fig. 6. The specimen temperature was lowered continuously at a cooling rate of 1 and 10 deg/min, and the images were acquired continuously with exposure time of 1–2 seconds under fixed defocus condition. High-density domains became visible at a few degrees below T_c as the temperature decreased (Fig. 6) [21]. We found that the DWs continued moving slightly below T_c and slowed down as temperature decreased. In other words, DW creep occurred. Interestingly, the domain evolution depended on the cooling rate. Figs. 6(a)–6(e) and 6(f)–6(j) were obtained at $H = 0$ when this rate was 1 and 10 degree/min, respectively. The reason that the DWs were not observed immediately below T_c was not only that the magnetization was smaller than the instrumental sensitivity, but also that DW motion was so fast that it could not be resolved with our instrumental time resolution. Coalescence and elapse of domains occurred as temperature decreased as a result of such DW motion. Finally, the domain structure came to be stationary below approximately 160 K.

A series of pictures for a cooling rate of 1 degree/min was obtained by accumulating five successive images with 2 seconds of exposure [Figs. 6(a)–6(e)]. No DW contrast was seen at 173 K [Fig. 6(a)]. A mixture of round bubble domains and chainlike domains became visible at 172 K [Fig. 6(b)]. The obtained images indicate that the DWs were nearly static on a timescale 10 seconds in duration below 172 K. However, most of the small round-shaped domains

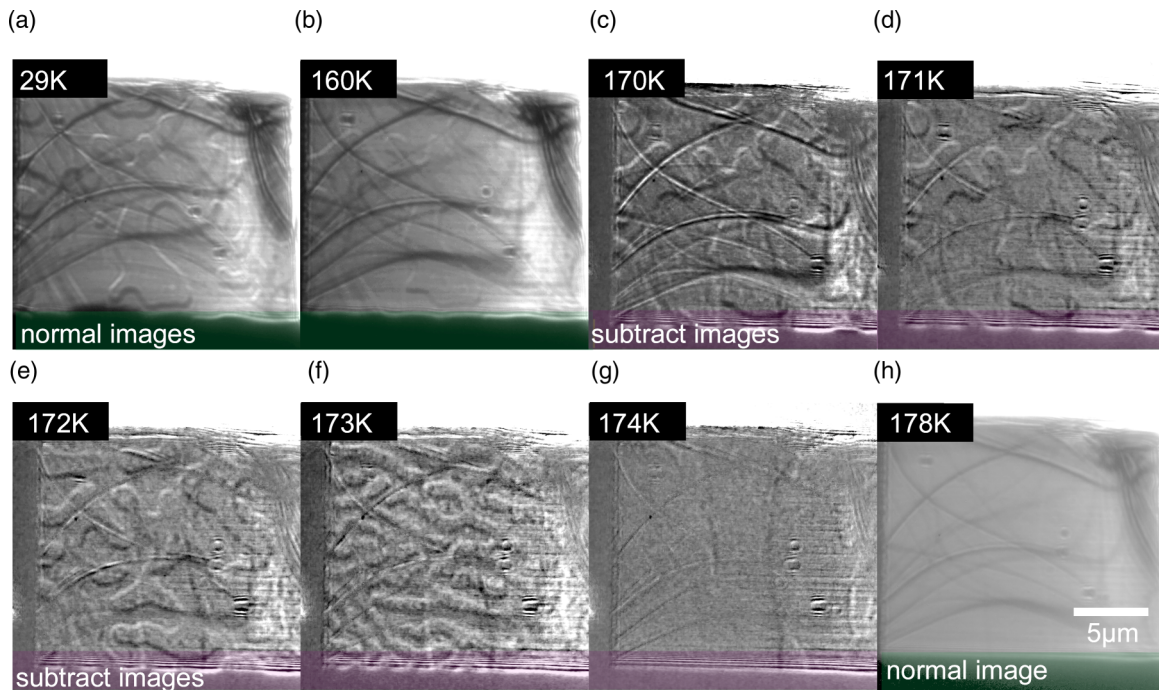


FIG. 5. Temperature-dependent magnetic domain evolution at $H = 0$ when heated through T_c . Spontaneous domain reorganization occurred just below T_c . We performed image subtraction between images obtained at (c)170–(g) 174 K and one with no magnetic contrast acquired at (h) 178 K to eliminate influence of bend contours and thickness variation within the specimen.

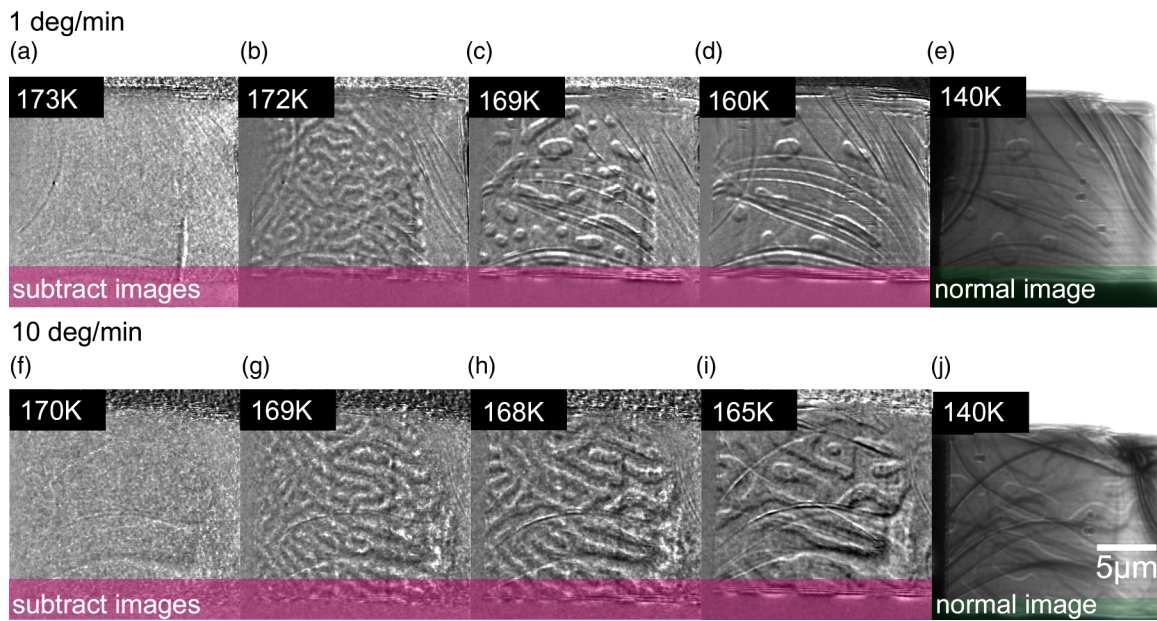


FIG. 6. Domain evolution at $H = 0$ when cooled through T_c . Domain creep occurred, hence domain structure varied when specimen cooling rate was [(a)–(e)] 1 deg/min and [(f)–(j)] 10 deg/min.

shrunk and disappeared, while a part of the adjacent domains coalesced as temperature decreased on a timescale of minutes. High-density domains were observed only in a narrow range, $172\text{ K} > T > 169\text{ K}$ [Figs. 6(b) and 6(c)]. Consequently, the large round-shaped bubble domains that minimized the DW area remained at 163 K [Fig. 6(d)]. V_r was 0.65 soon after the DW contrast became visible at 172 K, but it decreased

down to 0.16 at 161 K. Cooling through T_c at $H = 0$ is a usual procedure for obtaining thermally demagnetized domain structures. The present fraction is, however, much smaller than 0.5, which means the net magnetization reversed. When the specimen was cooled down very slowly, it took a single domain state occasionally as a result of the DWs being swept out from the specimen. There are several possible reasons for

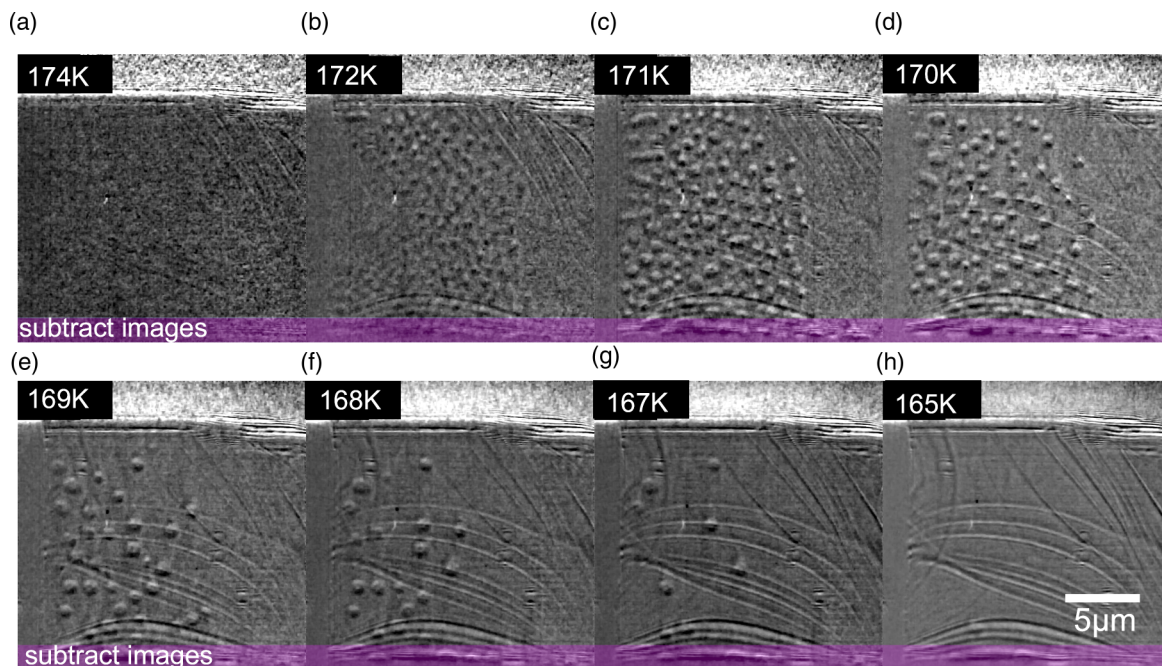


FIG. 7. Domain evolution at $H = 10\text{ Oe}$ when cooled through T_c . There was no domain at (a) 174 K. The high-density round-shaped domains were visible at (b) 172 K. The domain reorganization also occurred at (c) 171 K. The domain density decreased as the temperature decreased at (d) $170\text{ K} < T <$ (g) 167 K. The domains disappeared at (h) 165 K. Individual images were obtained by averaging 5 images with 1 second exposure.

the reversal: (1) the domain wall area decreases monotonically to decrease domain wall energy. The demagnetization energy is thought to be a negligible micromagnetic factor when the magnetization is extremely small immediately below T_c . (2) the coercivity of the specimen may be smaller than the residual stray field from the objective lens (< 1 Oe), although we have not measured the coercivity at the temperature range. (3) The equilibrium domain size is larger than the specimen size. We might observe multi domain with V_r nearly 0.5 if we could have observed specimens with large area.

Figures 6(f)–6(j) were obtained at $H = 0$ when the cooling rate was 10 degree/min. Half-size images were acquired continuously with 3-second exposures to record such fast DW motion, although image quality was degraded. Note that the specimen temperature may have been a little higher than the sensor read-out because the response of the holder was not fast enough. Although the direct comparison of temperature between the series of 1 and 10 deg/min is probably inappropriate, it is worthful to discuss the morphological evolution of domain shape in each series. The domains became visible at 169 K as shown in Fig. 6(g), while Compared with Fig. 6(b), the present domains are mostly chainlike-shaped. The domain density decreased as the temperature decreased, whereas the domains kept a chainlike shape as shown in Figs. 6(g)–6(i). Furthermore, V_r was 0.54 at 165 K, which was reasonable as a thermally demagnetized state. DW motion rarely occurred when $T < 160$ K as in with slow cooling.

The similar domain formation also occurred at $H = 10$ Oe (Fig. 7). The cooling rate was 1.3 deg/min. We did not examine the cooling rate dependence for this H . As the specimen was cooled down across T_c , round bubble domains became visible at (b) 172 K. The domain shape was different from those obtained at $H = 0$ (Fig. 6). The domain density decreased with keeping their round shapes, mainly because the small round domains collapsed as the temperature decreased [Figs. 7(b)–7(g)]. The finite field may help the individual domains to keep their shape with minimum DW area. Finally, the domain disappeared at (h) 165 K. However, it should be noted again that no DWs were observed during cooling at $H > 100$ Oe.

The characters of the high-density domains (occurring only slightly below T_c and at low external field, and being dominated by slow spin dynamics) agree with that of A state. However, the continuous DW motion and weak Lorentz contrast (magnetic phase change) due to small M_s at the temperature prevent us to determine the detailed spin configuration of such high-density domains.

IV. DISCUSSION

For comparison, macroscopic M - T curves obtained by bulk SQUID measurement (originally shown in Fig. 2 of Ref. [7]) were replotted as $(M/M_s + 0.5)$ - T curves by using Eq. (1) (Fig. 8). When the $(M/M_s + 0.5)$ takes the value 0 or 1, the specimen takes the single domain state. In the original figure, the ‘‘humps’’ and ‘‘dips’’ were observed on individual FC and ZFC curves at low H , respectively. The region surrounded by T_A (hump temperature depending on H) and T_c was assigned to the A-phase on the H - T magnetic phase diagram [7]. On the other hand, the latter dip occurred

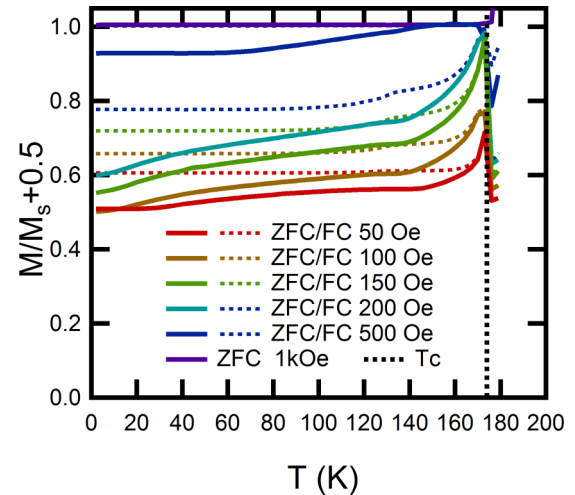


FIG. 8. Temperature- and external-field dependence of $M/M_s + 1/2$ obtained by bulk SQUID measurement, which is expected to be equivalent to volume fraction of domains with positive polarization.

between T_c and T_A . The ZFC curves matched the FC curves only at $H = 1000$ Oe, probably because the single domain state was kept for whole temperature range in both cases. The FC curve at 1000 Oe is therefore assumed to represent the temperature dependence of M_s , which was used to calculate M/M_s . Since we did not observe domain structure at $T > T_c$, negative slope above T_c is out of coverage of this study.

The $(M/M_s + 0.5)$ curves indicate that the DWs were involved in the bulk during cooling when $H \leq 500$ Oe. The curves exhibited rapid decrease just below T_c as the temperature decreased when the specimen was cooled down across T_c at $H \leq 200$ Oe, whereas it was nearly unity at $H \geq 500$ Oe. Their slopes decreased with decreasing the temperature, and subsequently became nearly constant at low temperature range. The transition between the two temperature zones occurred at T_A [7]. If the variation of M/M_s was ascribed to the DWs, their motion occurred to decrease M/M_s , and subsequently it was deactivated as the temperature decreased. The behavior of M/M_s at $T_A \leq T \leq T_c$ was surprising, because the volume of domains with magnetization *antiparallel* to H increased as the temperature decreased. The result suggests unusual competition between the DW, magnetostatic and Zeeman energies.

In the present study, we observed three different types of domain evolution during cooling through T_c depending on H .

(1) At $H = 0$, high-density bubble domains nucleated immediately below T_c . The coalescence and elapse of domains occurred according to the DW creep motion. The domain structure after the DW motion was deactivated below 160 K was dependent of cooling rate. Multidomain structure was quenched successfully down to 10 K only when the cooling rate was high, where the V_r was nearly 0.5. In contrast, the V_r approached to zero (or unity) as the temperature decreased slowly. The reason for the maze domain formation when quenched was that DW motion was deactivated during rapid cooling before the domains recovered a low-energy round shape. Accordingly, the domain evolution depends on temperature, field, and time. It is analogous to difference between

growth morphology and equilibrium shape of crystals. The energy-minimized equilibrium shape is quickly recovered when the surface diffusion is sufficiently high, whereas the deviation remains large when the surface diffusion is slow. The domain evolution was possibly influenced by the elimination of metastability during heating. The result cannot be directly compared with a bulk M - T curve, because bulk measurement cannot be performed at $H = 0$. An unusual ZFC curve measured at 2.5 Oe starting from nonnegligible negative magnetization was reported in Fig. S4 of Ref. [10], which may be due to the slow cooling rate.

(2) At $H = 10$ Oe, high-density bubble domain formation also occurred. The DW motion was driven by not only thermal depinning but also external field. The domain disappeared during cooling down to 160 K. The V_r increased up to unity as the temperature decreased. Such behavior was not observed in the bulk M/M_s measurement;

(3) At $H \geq 100$ Oe, no DW formation was observed. One possibility is that the single domain state was established during the ferromagnetic phase transition. Another possibility is that the multi-domain formation occurred during the phase transition, and the DWs were swept out because the DW pinning sites were not strong enough to pin the DWs under such large field and thermal fluctuation. It was impossible to determine which type of domain formation occurred because the DW contrast (if existed) was very weak when M_s was extremely small at such high temperature.

As a result, we did not observe that the V_r converged to constant values in between 0.5 and 1 as a function of H as the temperature decreased. Accordingly, the hump temperature T_A was not determined as a function of H . Therefore the A phase could not be assigned on the H - T magnetic phase diagram in the same manner as determined from the bulk M - T curves.

The heating behavior of the ZFC specimens is discussed next. It should be noted that the observation during heating at $H > 100$ Oe (Figs. 1–3) and at $H = 0$ (Fig. 5) was performed for the specimen of which initial maze domain was configured through quenching across T_c at $H = 0$. Since the DWs were fixed in the absence of driving field, the DWs are thought to be pinned by shallow pinning centers in such specimens. Therefore the domain evolution during heating such specimens might be determined not only by given temperature and field, but also by metastability. In the present study, we observed two different type of domain evolution during heating through T_c depending on H :

(1) At $H = 0$, DW motion was rarely observed up to 171 K, however, the spontaneous refinement of the domain occurred above 172 K. The domain reorganization is thought to be caused by the DW creep occurring near T_c . This is a reverse process of the domain coarsening during cooling at $H = 0$, too. The domain structure can be temperature-dependent through changes in micromagnetic parameters such as M_s , A , and K_u even when the external field driving DW motion is absent. Interestingly, the DW area increased as a result of the spontaneous domain refinement, whereas the DW motion occurred to reduce the DW area especially below 100 K in Figs. 1–3. The competition between demagnetization and DW energies is suggested to be quite different at low temperature (below 100 K) and slightly below T_c . Since such

micromagnetic parameters varies slowly with temperature, one may expect that domain reorganization should occur over wide temperature range. On the contrary, the drastic domain reorganization occurred in a quite narrow temperature range, slightly higher than the DW depinning temperature for $H = 100$ Oe (Fig. 3). The result suggests that the metastable domain configuration remained frozen while the DWs were effectively pinned during heating up to 171 K. The domain reorganization was triggered by the thermal depinning of the DWs to recover the energy-minimum configuration.

(2) At $H \geq 100$ Oe. The bulk $(M/M_s + 0.5)$ of the ZFC specimen (solid lines) increased when the H increased at 2 K. The result indicates the DW motion occurred responding to the increase of H . In the present domain observation, we did not observe significant DW motion when H increased at 10–12 K. The DWs were thought to be pinned more strongly in the TEM specimen. When the bulk specimen was heated up in given field, the $(M/M_s + 0.5)$ curves exhibited a moderate increase in the low temperature range, slow increase in the middle temperature range, and rapid increase in the high temperature range as the temperature increased up to T_c . The transition between middle to high temperature range corresponds to the dip in the original M - T diagram. The rapid increase in $(M/M_s + 0.5)$ in the high temperature range was quite similar to the rapid increase in the V_r curves above the depinning temperature (Fig. 4). Therefore the depinning temperatures corresponds to the dip temperature in the original figure.

The split between ZFC and FC curves can be explained in terms of the difference in the nature of pinning centers, thermal depinning, and DW motion driven by the external field. When the specimen was cooled at hundreds of oersted, the DWs were not easily pinned near T_c due to large thermal fluctuation. The pinning came to occur as the thermal fluctuation decreases as the temperature decreases. In such cases the DW pinning was thought to have occurred at the deep pinning centers preferentially. Once the DWs were pinned by such deep centers that were capable of capturing DWs under a strong thermal fluctuation and external field, the depinning rarely occur when the fluctuation decreases as the temperature decreases. The density of such pinning centers is expected to decrease as H increases. Therefore the M/M_s becomes constant (as a function of H) during further cooling at low temperature in the FC curves. To the contrary, the DWs were thought to have been pinned also by weaker pinning centers when the specimens were cooled in a weak field (including ZFC). Therefore depinning of such weakly pinned DWs is thought to occur even when the field was increased at 2 K, and the temperature increased under the low external field range in the bulk, although such behavior was not observed in the TEM observation. The disagreement between the TEM specimens and the bulk may be due to the pinning associated with surface and ion-induced defects. Another possibility for the differences is that the number of the domains in the restricted volume of the TEM specimen was so small that satisfactory statistics comparable to the bulk curves may not be obtained. We might obtain better agreement if we could have observed specimens with large area.

Although the occurrence of the A phase was not mapped on the H - T diagram in the present study, the characteristic

domain structure at low field and high temperature below T_c was formation and reorganization of fine-scale bubble domains according to the DW creep. The DW creep may be a reason for the slow spin dynamics because it delays the response of magnetization to a varying field. The present result suggests that continuous transition between the domain states at low- and high-temperature ranges was disturbed by the strong DW pinning. The continuous DW motion and weak Lorentz contrast (magnetic phase change) due to small M_s at the temperature prevented us to determine the detailed spin configuration of such high-density domains. Their structure does not seem to be topologically-protected, at least in the present size scale, field, and temperature. The topological protection may occur in different conditions such like very low field (e.g., $0 \text{ Oe} < H < 10 \text{ Oe}$).

The observed domain evolution was different from those reported for other materials in the previous studies. Although similar thermal depinning of DWs and magnetic viscosity was reported for a single-crystal $\text{BaFe}_{12}\text{O}_{19}$ with strong uniaxial anisotropy, it occurred in a temperature range far below T_c [22]. The present result was also quite different from that of another kagome ferromagnet, Fe_3Sn_2 , probably because the nonrigid uniaxial anisotropy of Fe_3Sn_2 depends on temperature [14,15]. Uniaxial anisotropy along the c axis of the $\text{Co}_3\text{Sn}_2\text{S}_2$ is quite stable for wide temperature ranges, as evidenced by the anisotropy field greater than 5 tesla even at

174 K [10]. A group of materials exhibiting similar behaviors such like the DW creep [23] may be found according to the research progress on magnetic texture occurring immediately below T_c . Further experiment is in plan to elucidate dynamic magnetic textures immediately below T_c of various uniaxial ferromagnets including $\text{Co}_3\text{Sn}_2\text{S}$ in high resolution by means of high-sensitivity, high-speed image acquisition using a direct camera [24].

V. CONCLUSION

The variation in magnetic domain structure within $\text{Co}_3\text{Sn}_2\text{S}_2$ was presented as a function of temperature, external field, and cooling rate. Bulk M - T curves were interpreted using temperature-dependent DW motions: DW pinning effective at low temperature, thermal depinning occurring as temperature increased, and DW creep just below T_c ascribed to slow spin dynamics. We consider that the occurrence of the A phase is due to formation of high-density bubble domains and their spontaneous reorganization according to the DW creep at low field and below T_c .

ACKNOWLEDGMENT

The authors would like to thank I. Kézsmárki, H. Shinada, and I. Kitagawa for the helpful discussion.

-
- [1] P. Vaquero and G. G. Sobany, *Sol. Stat. Sci.* **11**, 513 (2009).
- [2] W. Schnelle, A. Leithe-Jasper, H. Rosner, F. M. Schappacher, R. Pöttgen, F. Pielhofer, and R. Wehrich, *Phys. Rev. B* **88**, 144404 (2013).
- [3] M. Holder, Yu. S. Dedkov, A. Kade, H. Rosner, W. Schnelle, A. Leithe-Jasper, R. Wehrich, and S. L. Molodtsov, *Phys. Rev. B* **79**, 205116 (2009).
- [4] M. A. Kassem, Y. Tabata, T. Waki, and H. Nakamura, *J. Phys. Soc. Jpn.* **85**, 064706 (2016).
- [5] M. A. Kassem, Y. Tabata, T. Waki, and H. Nakamura, *J. Cryst. Growth* **426**, 208 (2015).
- [6] M. A. Kassem, Y. Tabata, T. Waki, and H. Nakamura, *J. Solid State Chem.* **233**, 8 (2016).
- [7] M. A. Kassem, Y. Tabata, T. Waki, and H. Nakamura, *Phys. Rev. B* **96**, 014429 (2017).
- [8] Q. Xu, E. Liu, W. Shi, L. Muechler, J. Gayles, C. Felser, and Y. Sun, *Phys. Rev. B* **97**, 235416 (2018).
- [9] Q. Wang, Y. Xu, R. Lou, Z. Liu, M. Li, Y. Huang, D. Shen, H. Weng, S. Wang, and H. Lei, *Nat. Commun.* **9**, 3681 (2018).
- [10] E. Liu, Y. Sun, N. Kumar, L. Muechler, A. Sun, L. Jiao, S.-Y. Yang, D. Liu, A. Liang, Q. Xu, J. Kroder, V. Süß, H. Borrmann, C. Shekhar, Z. Wang, C. Xi, W. Wang, W. Schnelle, S. Wirth, Y. Chen, S. T. B. Goennenwein, and C. Felser, *Nat. Phys.* **14**, 1125 (2018).
- [11] W. Yan, X. Zhang, Q. Shi, X. Yu, Z. Zhang, Q. Wang, S. Li, and H. Lei, *Solid State Commun.* **281**, 57 (2018).
- [12] N. Nagaosa and Y. Tokura, *Nat. Nanotechnol.* **8**, 899 (2013).
- [13] X. Yu, M. Mostovoy, Y. Tokunaga, W. Zhang, K. Kimoto, Y. Matsui, Y. Kaneko, N. Nagaosa, and Y. Tokura, *Proc. Natl. Acad. Sci. USA* **109**, 8856 (2012).
- [14] Z. Hou, W. Ren, B. Ding, G. Xu, Y. Wang, B. Yang, Q. Zhang, Y. Zhang, E. Liu, F. Xu, W. Wang, G. Wu, X. Zhang, B. Shen, and Z. Zhang, *Adv. Mater.* **29**, 1701144 (2017).
- [15] L. A. Fenner, A. A. Dee, and A. S. Wills, *J. Phys.: Condens. Matter* **21**, 452202 (2009).
- [16] D. R. Wicker, T. Suzuki, C. Jozwiak, A. Bostwick, E. Rotenberg, D. C. Bell, L. Fu, R. Comin, and J. G. Checkelsky, *Nature* **555**, 639 (2018).
- [17] A. Hubert and R. Schafer, *Magnetic Domains: The Analysis of Magnetic Microstructures* (Springer-Verlag, Berlin, Heidelberg, 1998).
- [18] T. Kawasaki, T. Yoshida, T. Matsuda, N. Osakabe, A. Tonomura, I. Matsui, and K. Kitazawa, *Appl. Phys. Lett.* **76**, 1342 (2000).
- [19] A. Sugawara, T. Akashi, P. D. Brown, R. P. Campion, T. Yoshida, B. L. Gallagher, and A. Tonomura, *Phys. Rev. B* **75**, 241306(R) (2007).
- [20] K. Harada, J. Endo, N. Osakabe, and A. Tonomura, *e-J. Surf. Sci. Nanotech.*, **6**, 29 (2008).
- [21] See Supplemental Material 1 at <http://link.aps.org/supplemental/10.1103/PhysRevMaterials.3.104421> for the full image sets of the corresponding observation and the image subtraction procedure.
- [22] X. X. Zhang, J. M. Hernandez, J. Tejada, R. Sole, and X. Ruiz, *Phys. Rev. B* **53**, 3336 (1996).
- [23] L. Peng, Y. Zhang, L. Ke, T.-H. Kim, Q. Zheng, J. Yan, X.-G. Zhang, Y. Gao, S. Wang, J. Cai, B. Shen, R. J. McQueeney, A. Kaminski, M. J. Kramer, and L. Zhou, *Nano Letters* **18**, 7777 (2018).
- [24] T. Tanigaki, T. Akashi, A. Sugawara, K. Miura, J. Hayakawa, K. Niitsu, T. Sato, X. Yu, Y. Tomioka, K. Harada, D. Shindo, and H. Shinada, *Sci. Rep.* **7**, 16598 (2017).